THE JOURNAL OF PHYSICAL CHEMISTRY C

Article

Cite This: J. Phys. Chem. C 2019, 123, 2031−2036

pubs.acs.org/JPCC

Theoretical and Experimental Study of (Ba,Sr)TiO_3 Perovskite Solid Solutions and $BaTiO_3$/$SrTiO_3$ Heterostructures

Leonid L. Rusevich,*[,†] Guntars Zvejnieks,[†] Eugene A. Kotomin,[†] Marjeta Maček Kržmanc,[‡] Anton Meden,[§] Špela Kunej,[‡] and Ioana D. Vlaicu[∥]

[†]Institute of Solid State Physics, University of Latvia, 8 Kengaraga Street, Riga LV-1063, Latvia

[‡]Advanced Materials Department, Jožef Stefan Institute, Jamova 39, Ljubljana 1000, Slovenia

[§]Faculty of Chemistry and Chemical Technology, University of Ljubljana, Večna pot 113, Ljubljana 1001, Slovenia

[∥]National Institute of Materials Physics, 405A Atomistilor Street, Magurele 077125, Ilfov, Romania

ABSTRACT: The results of experimental and theoretical ab initio study of structural and piezoelectric properties of (Ba,Sr)TiO_3 perovskite solid solutions are discussed and compared. Experimentally, plate-like (Ba,Sr)TiO_3 particles were synthesized by the topochemical conversion in the molten salt from $Bi_4Ti_3O_{12}$ template plates. All dimensions (side length ≈1 μm, thickness ≈200−400 nm) were well above the critical size necessary for observation of piezo- and ferroelectricity. The first-principles computations of the structural and electromechanical properties of solid solutions were performed with the CRYSTAL14 computer code within the linear combination of atomic orbitals approximation, using three advanced hybrid functionals of density functional theory. Different chemical compositions are considered for the ferroelectric and paraelectric phases. The calculated structural properties of solid solutions in tetragonal and cubic phases are in very good agreement with experimental data. Experimentally obtained and calculated band gaps are compared for cubic $SrTiO_3$ and tetragonal $BaTiO_3$. $BaTiO_3$/$SrTiO_3$ heterostructures were considered theoretically for different chemical compositions. The calculated piezoelectric properties of solid solutions and heterostructures in the ferroelectric phase are compared. It is predicted that both solid solutions and heterostructures improve the piezoelectric properties of bulk $BaTiO_3$, but solid solutions are more preferable for equal Sr concentrations.

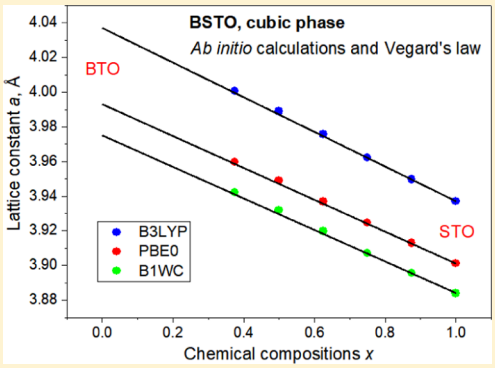

INTRODUCTION

Nowadays, the development of devices for energy storage applications and for harvesting and mutual transformations of mechanical and electrical energies is of great interest. In this respect, the utilization of piezoelectricity is an efficient way,[1] and, therefore, ferroelectric perovskites are important materials for many technological applications. For a long time, lead-zirconate-titanate (PZT) has been the most widely used piezoelectric material for electromechanical applications.[2,3] However, due to Pb toxicity, it is a challenging problem to develop lead-free ceramics with good piezoelectric properties. Recently, several lead-free piezoelectrics have been investigated.[4,5] $BaTiO_3$-based (BTO) piezoelectric materials are considered as potential substitution agents for PZT.[6,7] Most studies on biocompatible piezoelectrics have also focused on BTO-based materials.[8] Although pure BTO exhibits fairly low piezoelectric properties (and temperature stability of these properties) in comparison with PZT, further design could allow material improvement. This design may include domains, defects, phase boundary engineering, and texturing (see ref 6 and references therein). Functional properties of BTO-based materials are sensitive to chemical modifications. In particular, significant improvement of piezoelectric and dielectric properties was found in binary and ternary Sr-, Ca-, and Zr-modified BTO-based solid solutions.[6,9,10] To optimize the functional properties of BTO perovskite, $BaTiO_3$/$SrTiO_3$ (BTO/STO) ferroelectric plates (heterostructures) could also be used.[6,11]

At high temperatures, BTO has a cubic structure with Ti ions octahedrally coordinated with six nearest oxygen ions. It is a structure with centrosymmetric $Pm\bar{3}m$ space group (SG 221), and therefore, it is both paraelectric and nonpiezoelectric. As the temperature decreases, Ti ions are displaced from the cube center, which leads (at ambient pressure and at 393 K) to a paraelectric−ferroelectric and structural phase transition with spontaneous polarization directed parallel to the tetragonal edge of the pseudocubic unit cell. During this transition, crystal symmetry reduces from cubic (SG 221) to tetragonal (*P*4*mm*, SG 99). Upon further cooling, BTO undergoes two consecutive interferroelectric structural transitions: to orthorhombic phase (*Amm*2, SG 38) at 278 K and to rhombohedral phase (*R*3*m*, SG 160) below 183 K. Direction of spontaneous polarization at these transitions

Received: October 5, 2018
Revised: November 30, 2018
Published: January 1, 2019

DOI: 10.1021/acs.jpcc.8b09750
J. Phys. Chem. C 2019, 123, 2031−2036

reorients along a face diagonal (orthorhombic) and body diagonal (rhombohedral) of unit cell. All three phase transitions in BTO are of first-order.

An important aspect in the improvement of functional properties of materials is the possibility to perform computations of structural, electronic, and electromechanical properties of perovskites based on an ab initio (first-principles) approach. Several calculations of functional properties of BTO crystals have been reported.[12−14] Recently, we performed the first theoretical study of the electromechanical/piezoelectric properties of tetragonal $Ba_{(1-x)}Sr_xTiO_3$ (BSTO) ferroelectric solid solution by means of first-principles calculations.[15] Our calculations for chemical compositions x = 0.125 and 0.25 show that Sr doping of BTO enhances its piezoelectric properties.

As experimentally known,[16,17] at $x \approx 0.3$ (at room temperature), BSTO reveals phase transition from the tetragonal to cubic phase (i.e., ferroelectric−paraelectric transition), which means that for higher Sr concentrations, this solid solution has a cubic symmetry without piezoelectric properties. At the same time, BTO/STO heterostructures still remain ferroelectric even at high Sr concentration (see ref 18 and references therein). In this paper, the preparation and structural properties of complex BSTO perovskites are discussed. We analyze the structural parameters of tetragonal (the most important for applications) and cubic BSTO room temperature phases. Additionally, we theoretically considered BTO/STO heterostructures with the same chemical compositions as solid solutions in the ferroelectric phase ($x < 0.3$).

EXPERIMENTAL SECTION

Plate-like BSTO particles were synthesized using a two-stage reaction process in the molten salt. In the first step, $Bi_4Ti_3O_{12}$ plates were synthesized from Bi_2O_3 and TiO_2 nanopowders in the molten salt (NaCl/KCl = 1:1) at 800 °C for 2 h. In the second stage, these $Bi_4Ti_3O_{12}$ plate-like particles were used as the template for the preparation of BSTO plates via topochemical transformation in the molten salt with the following ratio of reagents: KCl/NaCl/$Bi_4Ti_3O_{12}$/($BaCO_3$ + $SrCO_3$) = 39:39:1:10. The reactions were performed at the following heat treatment conditions: heating 10 °C/min to 600 °C and 0.5 °C/min to 900 °C, isothermal annealing for 2 h at this temperature and cooling 1 °C/min to room temperature. Pure BSTO plates were obtained after the removal of salt by washing with water and elimination of side products by sedimentation and washing with HNO_3 (2 M). The final BSTO composition was tailored, based on the experimentally determined relationship between the Ba/Sr ratio in the initial reaction mixture and the Ba/Sr ratio in the formed perovskite plates. The synthesis procedure is described in detail in refs 19 and 20.

The morphology and actual composition of BSTO plate-like particles were investigated using a field-emission scanning electron microscope (JSM-7600 F, JEOL), equipped with an Oxford Instruments Inca energy-dispersive X-ray spectrometer (EDS). The unit cell parameters were determined from X-ray powder diffraction patterns, collected on a PANalytical X'pert PRO MPD X-ray powder diffractometer. Pure Cu $K\alpha_1$ radiation with λ = 1.5406 Å and high resolution were ensured by a Johansson type primary monochromator. Rietveld refinement was used to calculate the unit cell parameters. A tetragonal structure (SG 99, collection code 237105 from the ICSD database) was loaded into the program and only the background coefficients, profile parameters, and unit cell parameters were refined. The atomic coordinates were fixed, as well as the population parameters, which were calculated from the chemical composition, found by EDS. Profile R_{wp} showed good agreement in all cases (between 10 and 15%) and in the cases where the samples were actually cubic, this was clearly seen from the value of the c/a ratio, which was very close to 1 in such cases.

The optical band gaps for direct and indirect transitions in tetragonal BTO and cubic STO plate-like particles were determined from the diffuse reflectance spectra using the Kubelka−Munk method. Spectroscopic measurements were performed using a UV−vis−NIR spectrophotometer (Shimadzu UV-3600) equipped with an integrating sphere (ISR-3100, 60 mm, Shimadzu); $BaSO_4$ standard was used as the reference.

COMPUTATIONAL DETAILS

Computational details of our calculations are described in detail in our previous paper.[15] Here, we will outline only basic moments and specific details. The quantum chemical computer code CRYSTAL14 suitable for ab initio materials modeling[21] was used within the linear combination of atomic orbitals approximation of density functional theory. The small core effective pseudopotentials are used for Ba, Ti, and Sr atoms,[22] whereas an all-electron basis set is used for O atoms.[23] Calculations are performed with three commonly used hybrid exchange−correlation functionals.[24] One is PBE0,[25] where the Perdew−Burke−Ernzerhof (PBE) exchange functional is combined with 25% of Hartree−Fock (HF) exchange and the PBE correlation functional. The second is the B1WC functional,[26] which combines the Wu−Cohen WCGGA exchange functional with 16% of HF exchange and the Perdew−Wang PWGGA correlation functional. Finally, the third, B3LYP functional, is a three-parameter functional, combining the BECKE exchange functional with 20% of HF exchange and the Lee−Yang−Parr (LYP) correlation functional (NONLOCAL parameters are 0.9 and 0.81).[24]

A 2 × 2 × 2 supercell of the tetragonal (SG 99) or cubic (SG 221), depending on Sr concentration, BTO unit cell, is used as the computational model for the BSTO solid solution. This supercell consists of 40 atoms (8 primitive unit cells). In the supercell calculations, we modeled artificially ordered $Ba_{(1-x)}Sr_xTiO_3$ solid solutions using a series of different compositions (i.e., Sr/Ba ratio), where Ba atoms are progressively replaced by Sr atoms. With the tetragonal supercell, we considered three different Sr concentrations: pure BTO (without substitution, x = 0.0); one Ba atom is replaced with an Sr atom (x = 0.125); and two Ba atoms are replaced with Sr atoms (x = 0.25). The computations for six more Sr concentrations (x = 0.375, 0.5, ..., 1, where x = 1 is the case of pure STO) were performed with a cubic supercell according to the fact that for compositions with $x \geq 0.3$, BSTO solid solution has cubic symmetry. To preserve symmetry, for the x = 0.125 composition, we replaced the Ba atom at the coordinate origin (0, 0, 0), whereas, for x = 0.25, we replaced the first atom at the origin and the second with coordinates (0.5, 0.5, 0.5). In general, we have seven different possibilities for the substitution of the second atom. But, as was pointed in ref 15, the effect of configurational disorder (different configurations of atoms) on BSTO is small (less than 4% for the elastic properties, calculated by the PBE0 functional, and significantly less for structural properties), and therefore, we do not take into account this effect in the current work and

DOI: 10.1021/acs.jpcc.8b09750
J. Phys. Chem. C 2019, 123, 2031−2036

consider for $x = 0.25$ only one, mentioned above, configuration of atoms (see ref 15 for details). For the same reason, in cubic structures ($x > 0.3$), we only retain cubic symmetry in replacing Ba atoms with Sr atoms and restrict ourselves to a single configuration for each chemical composition.

The computational model for the BTO/STO heterostructure is the $1 \times 1 \times n$ supercell of the tetragonal (SG 99) BTO unit cell. Thus, we consider the superlattice $(BTO)_k/(STO)_l$, where k and l refer to the thickness (in unit cells) of BTO and STO layers, respectively, and $k + l = n$ (i.e., we replace in the supercell l of consecutive Ba atoms with Sr atoms). This superlattice is repeated along the z axis m times, i.e., it has a $[(BTO)_k/(STO)_l]_m$ structure; in our computations, $m = \infty$. To calculate heterostructures with the same chemical compositions, as in solid solutions ($x = 0.0$, 0.125, and 0.25), we used 8-layer ($n = 8$) structures—$(BTO)_8$, $(BTO)_7/(STO)_1$, and $(BTO)_6/(STO)_2$, respectively.

Computation of direct and converse piezoelectricity (using the Berry phase approach) is implemented in CRYSTAL14 as a fully automated procedure.[24]

RESULTS AND DISCUSSION

The composition of experimentally grown BSTO plate-like particles was found to be different from that expected from the $BaCO_3/SrCO_3$ ratio in the initial reaction mixture. Nevertheless, this topochemical conversion reaction is reasonable because all side products were possibly eliminated, enabling the preparation of pure perovskites with defined shape particles with negligible Bi remains (<0.9 atom %). Additionally, an arbitrary solid solution with $0 \le x \le 0.82$ ($0 \le x' \le 0.3$ in the initial reaction mixture) could be prepared based on the experimentally determined relationship $x \approx 2.7x'$ (see ref 20). A detailed analysis of the compositional dependence of the unit cell parameters, obtained by the Rietveld refinement of the room temperature X-ray diffraction patterns, revealed that unit cell volume nearly linearly decreases with an increase of Sr content. Similarly, the c/a ratio (characterizing tetragonal distortion) linearly decreases from 1.0092 ($x = 0$) to 1.0037 ($x = 0.23$) and then stabilized at $c/a = 1$ (cubic structure) for $0.23 < x \le 1$ (Table 1).

In contrast to $Ba_{(1-x)}Sr_xTiO_3$ with $0 \le x \le 0.11$, which exhibits clear tetragonal splitting and significant ferroelectric and piezoelectric characteristics as determined by differential scanning calorimetry (DSC) and piezoresponse force microscope (PFM) investigations, the composition with $x = 0.175$ showed a weak ferroelectric and piezoelectric response observed only by PFM but not by DSC. Although the composition with $x = 0.23$ exhibits some small tetragonality ($c/a = 1.0037$), no ferroelectric and piezoelectric effects were detected by PFM for this composition at room temperature.[20]

Before theoretical investigation of BSTO solid solutions, we calculated the lattice constants and band gaps for pure bulk BTO and STO crystals. The obtained results for the cubic (SG 221) phases of BTO and STO are given in Table 2, where they are compared also with experimental data, obtained in this study and taken from the literature.

Table 1. Experimental Dependence of Unit Cell Structural Parameters (Lattice Constants a, c and Volume V) of $Ba_{(1-x)}Sr_xTiO_3$ Plates, Obtained by the Topochemical Conversion, on Composition x[a]

x	a, Å	c, Å	c/a	V, Å^3
0	3.9983(1)	4.0352(1)	1.0092	64.507(3)
0.054	3.9937(1)	4.0271(1)	1.0084	64.230(3)
0.11	3.9872(1)	4.0144(1)	1.0068	63.821(3)
0.175	3.9817(1)	4.0027(1)	1.0053	63.459(3)
0.23	3.9756(1)	3.9904(1)	1.0037	63.071(3)
0.38	3.9656(1)	3.9630(1)	0.9993	62.324(3)
0.53	3.9511(1)	3.9504(1)	0.9998	61.671(3)
0.82	3.9218(1)	3.9215(1)	0.9999	60.315(3)
0.95	3.9092(1)	3.9096(1)	1.0001	59.744(3)
1	3.9065(1)	3.9053(1)	0.9997	59.597(3)

[a]Numbers in parentheses are standard deviations at the last given digit.

Table 2. Parameters of Cubic Phases of BTO and STO—Lattice Constant a and Band Gap E_g—Calculated Using Three Hybrid Functionals[a]

	PBE0	B1WC	B3LYP	expt
		BTO, SG 221		
a, Å	3.993	3.975	4.037	3.996[27]
E_g[b], eV	3.97 (4.00)	3.20 (3.24)	3.48 (3.55)	3.2[28]
		STO, SG 221		
a, Å	3.901	3.884	3.937	3.906;[c] 3.905[29]
E_g[b], eV	4.16 (4.47)	3.36 (3.68)	3.67 (3.98)	3.19 (3.33);[c] 3.25 (3.75)[30]

[a]Expt—experimental data. The experimental band gap[28] at a temperature ≈130 °C. [b]Indirect (direct) band gap. [c]This study.

As one can see from Table 2, for both the crystals, the PBE0 functional gives the best agreement with the experimental value for lattice constant a, whereas the B3LYP functional shows the worst agreement. For both BTO and STO in their cubic phases, calculations yield indirect band gaps. The band gaps, calculated by means of the B1WC functional, are very close to experimental data for both crystals.

The results of our calculations of structural properties and band gap for the BTO crystal in the tetragonal phase as well as direct (e_{33}) and converse (d_{33}) piezoelectric constants along with experimental data are given in Table 3.

Table 3 reveals that the B3LYP functional gives better agreement with experimental data for $a = b$ lattice constant but the worst for c constant and the tetragonal ratio c/a. At the same time, the B1WC functional gives the best agreement for c constant and for the c/a ratio (discrepancy with the experimental value is ~1%). Concerning the band gap, the B1WC functional gives again the result, which is closer to experimental data, and thus, we conclude that the B1WC functional reproduces correctly the experimental band gap (although it gives slightly overestimated values for band gaps in comparison with experimental data).

The origin of the piezoelectricity in BTO is related mainly to the atomic relaxations with a small electronic "clamped-ion" contribution.[15] For each piezoelectric tensor, direct and converse, we show in Table 3 only one constant, the most often defined in experiments. Table 3 demonstrates a considerable discrepancy between theory and experiments on piezoelectric constants. Note, however, that we performed calculations for a single domain crystal, whereas in real materials, the domain sizes and movement of domain walls can be by major factors, determining the piezoelectric properties of samples.[6] Therefore, the analysis should be concentrated on the general trend in the behavior of the piezoelectric constants.

DOI: 10.1021/acs.jpcc.8b09750
J. Phys. Chem. C 2019, 123, 2031−2036

Table 3. BTO Structural Properties, Band Gap, and Piezoelectric Constants (Tetragonal Phase, SG 99)

	PBE0	B1WC	B3LYP	expt
		Lattice Constants		
$a = b$, Å	3.971	3.962	3.991	3.998;[a] 3.992[27]
c, Å	4.131	4.050	4.292	4.035;[a] 4.036[27]
c/a	1.040	1.022	1.075	1.009;[a] 1.011[27]
		Band Gap		
E_g[b], eV	4.08 (4.52)	3.26 (3.60)	3.62 (4.18)	2.98 (3.23);[a] 3.38 (3.27)[28]
		Piezoelectric Constants		
e_{33}, C/m^2	3.3	4.2	2.6	6.7[31]
d_{33}, pm/V	37.0	32.7	57.3	85.6;[32] 90[33]

[a]This study. [b]Indirect (direct) band gap for calculated and experimental values, obtained in this study; experimental data[28] at room temperature for light polarized parallel (perpendicular) to the ferroelectric c axis.

On the basis of our theoretical calculations by three functionals for three Sr concentrations (x = 0.0, 0.125, and 0.25) and experimental data (Table 1), for the tetragonal phase of BSTO, dependences c/a vs x and V (unit cell volume) vs x are plotted in Figures 1 and 2, respectively.

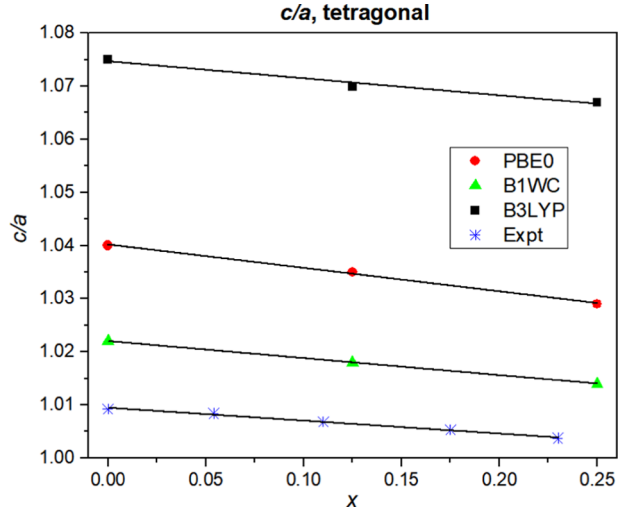

Figure 1. Theoretical and experimental dependences of tetragonal ratio c/a vs chemical compositions x (Sr doping) for the tetragonal phase of BSTO. The lines demonstrate linear fitting.

As one can see in Figure 1, close to the linear dependences of c/a vs x (Sr concentration) are both theoretical and experimental results (R-squared displacement for experimental data is 0.9937, for PBE0, B1WC, and B3LYP functionals—0.9973, 1.0, and 0.9796, respectively); theoretical data are overestimated for all functionals; the best agreement with experiment (for c/a and slope) is demonstrated by the B1WC functional.

Similar analysis for the volume of unit cell (Figure 2) reveals again dependences that are close to linear ($\langle R^2 \rangle$ for experimental data is 0.9975, 1—for PBE0 and B1WC functionals and 0.9997—for the B3LYP functional) and demonstrates very good agreement between experimental and theoretical data; the PBE0 functional shows the best agreement with experiment.

Let us consider now the cubic phase of BSTO solid solution (observed experimentally at high Sr concentrations, $x > 0.3$). Using theoretical calculations with three functionals for the cubic phase and the experimental data (Table 1), dependences a (lattice constant) vs x are plotted in Figure 3.

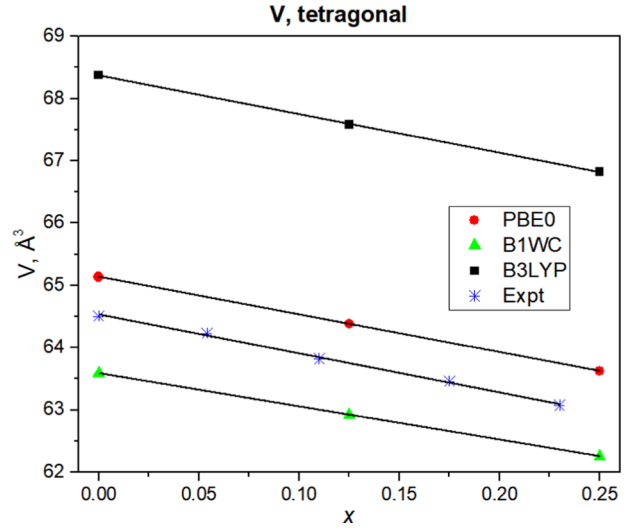

Figure 2. Theoretical and experimental dependences of unit cell volume V vs chemical compositions x for the tetragonal phase of BSTO. The lines demonstrate linear fitting.

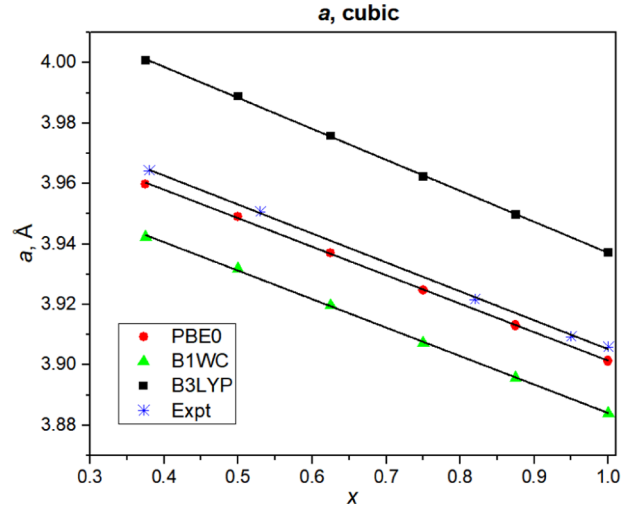

Figure 3. Theoretical and experimental dependences of lattice constant a vs chemical compositions x for the cubic phase of BSTO. The lines demonstrate linear fitting.

One can see the linear dependence a vs x for both theoretical and experimental data; these dependences are fulfilled with high accuracy: $\langle R^2 \rangle$ for experimental data is 0.9993 and that for theoretical data is within the range of

DOI: 10.1021/acs.jpcc.8b09750
J. Phys. Chem. C 2019, 123, 2031−2036

Table 4. Piezoelectric Constants for BTO/STO Heterostructures and BSTO Solid Solutions, Calculated by the PBE0 Functional[a]

	BTO/STO heterostructures				
	$(BTO)_8$	$(BTO)_7/(STO)_1$	%	$(BTO)_6/(STO)_2$	%
e_{33}, C/m^2	3.295	3.564	8.2	3.841	16.6
d_{33}, pm/V	36.992	37.838	2.3	38.518	4.1
	BSTO solid solutions				
	$x = 0$	$x = 0.125$	%	$x = 0.25$	%
e_{33}, C/m^2	3.294	3.720	12.9	4.270	29.6
d_{33}, pm/V	36.987	39.594	7.0	42.404	14.6

[a]%—gain of piezoelectric constants with regard to pure BTO systems ($(BTO)_8$ or $x = 0$).

0.9995−0.9997. Note the excellent agreement between calculated and experimental data; in particular, the PBE0 functional shows remarkable coincidence with the experiment (the difference between experimental and theoretical values a is ∼0.1%). On the basis of theoretical computations of the BSTO cubic structure, we found very accurate implementation of Vegard's law for the lattice constant a of the cubic phase of BSTO, calculated by all three functionals.

Finally, let us discuss the piezoelectric constants of BSTO solid solutions and BTO/STO heterostructures calculated for different compositions. We compare their piezoelectric properties for identical dopant concentrations $0 \leq x \leq 0.25$ when solid solutions show piezoelectric properties (more detailed general study of the heterostructures will be published separately). The results, calculated using the PBE0 functional, for heterostructures and solid solutions with the same chemical compositions (Sr/Ba ratio ≤0.25) are given in Table 4. $(BTO)_8$ for heterostructures and $x = 0$ for solid solutions are different ways of calculation of bulk BTO, and thus, the results have to be identical; Table 4 reveals this with high accuracy.

One can see from Table 4 that piezoelectric constants demonstrate growth upon substitution of Ba with Sr atoms both for solid solutions and for heterostructures but solid solutions are more preferable at considered Sr concentrations. Indeed, for solid solutions at $x = 0.25$, we see enhancement (in comparison with $x = 0$) of e_{33} and d_{33} piezoelectric constants by 30 and 15%, respectively, and only by 17% (e_{33}) and 4% (d_{33}) for heterostructures. The same trend remains in calculations with the B1WC functional.

CONCLUSIONS

A-site-substituted ($ATiO_3$) complex perovskite BSTO plate-like particles were synthesized by a topochemical conversion reaction in molten salt. The relationship between the actual and proposed Sr concentrations was determined. The experimental study was focused on the examination of the structural properties of the BSTO particles depending on chemical composition x. Moreover, optical band gaps for the cubic phase of STO and the tetragonal phase of BTO were measured. The results of the experimental and theoretical studies of the structural changes in BSTO solid solutions with different Sr concentrations (for tetragonal and cubic phases) agree very well with each other for the lattice constants, volumes, and tetragonality parameter c/a. This demonstrates that the synthesized plate-like particles are large enough to be considered as nearly bulk materials. We have shown that both the PBE0 and B1WC hybrid functionals are quite suitable for the description of structural parameters of BSTO for different chemical compositions and the B1WC functional gives the best results for the band gaps.

It is theoretically predicted that both solid solutions and heterostructures improve the piezoelectric properties of bulk BTO but solid solutions in their ferroelectric phase are more efficient than heterostructures for the same Sr concentrations.

AUTHOR INFORMATION

Corresponding Author

*E-mail: leorus@inbox.lv. Phone: +371-67187480.

ORCID

Leonid L. Rusevich: 0000-0002-4030-6157
Eugene A. Kotomin: 0000-0002-8122-6276
Marjeta Maček Kržmanc: 0000-0003-3436-5692

Notes

The authors declare no competing financial interest.

ACKNOWLEDGMENTS

This study was supported by the ERA-NET HarvEnPiez project. The authors would like to thank their national funding agencies (Latvian State Education Development Agency, Slovenian Ministry of Higher Education, Science and Technology, Romanian National Authority for Scientific Research and Innovation, CCCDI-UEFISCDI, project number 49/2016 within PNCDI III—M-ERA NET Program).

REFERENCES

(1) Bowen, C. R.; Kim, H. A.; Weaver, P. M.; Dunn, S. Piezoelectric and Ferroelectric Materials and Structures for Energy Harvesting Applications. *Energy Environ. Sci.* **2014**, *7*, 25−44.

(2) Jaffe, B.; Cook, W. R.; Jaffe, H. *Piezoelectric Ceramics*; Academic Press: London, 1971.

(3) Damjanovic, D. Ferroelectric, Dielectric and Piezoelectric Properties of Ferroelectric Thin Films and Ceramics. *Rep. Prog. Phys.* **1998**, *61*, 1267−1324.

(4) Rödel, J.; Jo, W.; Seifert, K. T. P.; Anton, E.-M.; Granzow, T.; Damjanovic, D. Perspective on the Development of Lead-Free Piezoceramics. *J. Am. Ceram. Soc.* **2009**, *92*, 1153−1177.

(5) Mahajan, A.; Zhang, H.; Wu, J.; Ramana, E. V.; Reece, M. J.; Yan, H. Effect of Phase Transitions on Thermal Depoling in Lead-Free $0.94(Bi_{0.5}Na_{0.5}TiO_3)$-$0.06(BaTiO_3)$ Based Piezoelectrics. *J. Phys. Chem. C* **2017**, *121*, 5709−5718.

(6) Acosta, M.; Novak, N.; Rojas, V.; Patel, S.; Vaish, R.; Koruza, J.; Rossetti, G. A., Jr.; Rödel, J. $BaTiO_3$-Based Piezoelectrics: Fundamentals, Current Status, and Perspectives. *Appl. Phys. Rev.* **2017**, *4*, No. 041305.

(7) Gao, J.; Xue, D.; Liu, W.; Zhou, C.; Ren, X. Recent Progress on $BaTiO_3$-Based Piezoelectric Ceramics for Actuator Applications. *Actuators* **2017**, *6*, 24.

DOI: 10.1021/acs.jpcc.8b09750
J. Phys. Chem. C 2019, 123, 2031−2036

(8) Baxter, F. R.; Bowen, C. R.; Turner, I. G.; Dent, A. C. E. Electrically Active Bioceramics: A Review of Interfacial Responses. *Ann. Biomed. Eng.* **2010**, *38*, 2079−2092.
(9) Fu, D.; Itoh, M.; Koshihara, S. Crystal Growth and Piezoelectricity of $BaTiO_3$-$CaTiO_3$ Solid Solution. *Appl. Phys. Lett.* **2008**, *93*, No. 012904.
(10) Dong, L.; Stone, D. S.; Lakes, S. Enhanced Dielectric and Piezoelectric Properties of $x BaZrO_3$-$(1-x)BaTiO_3$ Ceramics. *J. Appl. Phys.* **2012**, *111*, No. 084107.
(11) Schlom, D. G.; Chen, L.-Q.; Eom, C.-B.; Rabe, K. M.; Streiffer, S. K.; Triscone, J.-M. Strain Tuning of Ferroelectric Thin Films. *Annu. Rev. Mater. Res.* **2007**, *37*, 589−626.
(12) Khalal, A.; Khatib, D.; Jannot, B. Elastic and Piezoelectric Properties of $BaTiO_3$ at Room Temperature. *Phys. B* **1999**, *271*, 343−347.
(13) Meng, X.; Wen, X.; Qin, G. DFT Study on Elastic and Piezoelectric Properties of Tetragonal $BaTiO_3$. *Comput. Mater. Sci.* **2010**, *49*, S372−S377.
(14) Mahmoud, A.; Erba, A.; El-Kelany, K. E.; Rerat, M.; Orlando, R. Low-Temperature Phase of $BaTiO_3$: Piezoelectric, Dielectric, Elastic, and Photoelastic Properties from *Ab Initio* Simulations. *Phys. Rev. B* **2014**, *89*, No. 045103.
(15) Rusevich, L. L.; Zvejnieks, G.; Erba, A.; Dovesi, R.; Kotomin, E. A. Electromechanical Properties of $Ba_{(1-x)}Sr_xTiO_3$ Perovskite Solid Solutions from First-Principles Calculations. *J. Phys. Chem. A* **2017**, *121*, 9409−9414.
(16) Lemanov, V. V.; Smirnova, E. P.; Syrnikov, P. P.; Tarakanov, E. A. Phase Transitions and Glasslike Behavior in $Sr_{1-x}Ba_xTiO_3$. *Phys. Rev. B* **1996**, *54*, 3151−3157.
(17) Kim, S. W.; Choi, H. I.; Lee, M. H.; Park, J. S.; Kim, D. J.; Do, D.; Kim, M. H.; Song, T. K.; Kim, W. J. Electrical Properties and Phase of $BaTiO_3$-$SrTiO_3$ Solid Solution. *Ceram. Int.* **2013**, *39*, S487−S490.
(18) Schlom, D. G.; Chen, L.-Q.; Fennie, C. J.; Gopalan, V.; Muller, D. A.; Pan, X.; Ramesh, R.; Uecker, R. Elastic Strain Engineering of Ferroic Oxides. *MRS Bull.* **2014**, *39*, 118−130.
(19) Kržmanc, M. M.; Jančar, B.; Uršič, H.; Tramšek, M.; Suvorov, D. Tailoring the Shape, Size, Crystal Structure, and Preferential Growth Orientation of $BaTiO_3$ Plates Synthesized Through a Topochemical Conversion Process. *Cryst. Growth Des.* **2017**, *17*, 3210−3220.
(20) Kržmanc, M. M.; Uršič, H.; Meden, A.; Korošec, R. C.; Suvorov, D. $Ba_{1-x}Sr_xTiO_3$ plates: Synthesis through Topochemical Conversion, Piezoelectric and Ferroelectric Characteristics. *Ceram. Int.* **2018**, *44*, 21406−21414.
(21) Dovesi, R.; Orlando, R.; Erba, A.; Zicovich-Wilson, C. M.; Civalleri, B.; Casassa, S.; Maschio, L.; Ferrabone, M.; De La Pierre, M.; D'Arco, P.; et al. CRYSTAL14: A Program for the *Ab Initio* Investigation of Crystalline Solids. *Int. J. Quantum Chem.* **2014**, *114*, 1287−1317.
(22) Piskunov, S.; Heifets, E.; Eglitis, R. I.; Borstel, G. Bulk Properties and Electronic Structure of $SrTiO_3$, $BaTiO_3$, $PbTiO_3$ Perovskites: An *Ab Initio* HF/DFT Study. *Comput. Mater. Sci.* **2004**, *29*, 165−178.
(23) Bredow, T.; Jug, K.; Evarestov, R. A. Electronic and Magnetic Structure of $ScMnO_3$. *Phys. Status Solidi B* **2006**, *243*, R10−R12.
(24) Dovesi, R.; Saunders, V. R.; Roetti, C.; Orlando, R.; Zicovich-Wilson, C. M.; Pascale, F.; Civalleri, B.; Doll, K.; Harrison, N. M.; Bush, I. J. et al. *CRYSTAL14 User's Manual*; University of Torino: Torino, Italy, 2014.
(25) Adamo, C.; Barone, V. Toward Reliable Density Functional Methods without Adjustable Parameters: The PBE0 Model. *J. Chem. Phys.* **1999**, *110*, 6158−6170.
(26) Bilc, D. I.; Orlando, R.; Shaltaf, R.; Rignanese, G. M.; Iniguez, J.; Ghosez, Ph. Hybrid Exchange-Correlation Functional for Accurate Prediction of the Electronic and Structural Properties of Ferroelectric Oxides. *Phys. Rev. B* **2008**, *77*, No. 165107.
(27) *Ternary Compounds, Organic Semiconductors*; Madelung, O.; Rössler, U.; Schulz, M., Eds.; Landolt-Börnstein — Group III Condensed Matter, Springer: Berlin, 2000; Vol. *41E*.
(28) Wemple, S. H. Polarization Fluctuations and the Optical-Absorption Edge in $BaTiO_3$. *Phys. Rev. B* **1970**, *2*, 2679−2689.
(29) Cao, L.; Sozontov, E.; Zegenhagen, J. Cubic to Tetragonal Phase Transition of $SrTiO_3$ under Epitaxial Stress: An X-Ray Backscattering Study. *Phys. Status Solidi A* **2000**, *181*, 387−404.
(30) van Benthem, K.; Elsässer, C.; French, R. H. Bulk Electronic Structure of $SrTiO_3$: Experiment and Theory. *J. Appl. Phys.* **2001**, *90*, 6156−6164.
(31) Zgonik, M.; Bernasconi, P.; Duelli, M.; Schlesser, R.; Günter, P.; Garrett, M. H.; Rytz, D.; Zhu, Y.; Wu, X. Dielectric, Elastic, Piezoelectric, Electro-Optic, and Elasto-Optic Tensors of $BaTiO_3$ Crystals. *Phys. Rev. B* **1994**, *50*, 5941−5949.
(32) Berlincourt, D.; Jaffe, H. Elastic and Piezoelectric Coefficients of Single-Crystal Barium Titanate. *Phys. Rev.* **1958**, *111*, 143−148.
(33) Davis, M.; Budimir, M.; Damjanovic, D.; Setter, N. Rotator and Extender Ferroelectrics: Importance of the Shear Coefficient to the Piezoelectric Properties of Domain-Engineered Crystals and Ceramics. *J. Appl. Phys.* **2007**, *101*, No. 054112.

DOI: 10.1021/acs.jpcc.8b09750
J. Phys. Chem. C 2019, 123, 2031−2036